

An analytical model for simulation of the wind field in a typhoon boundary layer

Yan Meng*, Masahiro Matsui, Kazuki Hibi

*Environmental Engineering Department, Institute of Technology, Shimizu Corporation, No. 4-17, Etchujima,
3-chome, Koto-ku, Tokyo 135, Japan*

Received 12 March 1994; accepted 13 May 1994

Abstract

An analytical model has been developed for calculating the wind field in a moving typhoon boundary layer. The present model has an upper inviscid layer of cyclostrophic balance and a lower friction layer controlled by a surface drag coefficient and eddy viscosity. Velocity in the inviscid region is described first, using the assumption that the wind field moves with the translation velocity of the typhoon. Perturbation analysis is then performed to obtain the tangential and radial boundary layer velocity in the friction region. Wind speeds and directions predicted by the present model agree favorably with observations obtained at a 100 m height tower during three typhoons in 1991. Rapid variations in wind speed due to surface roughness and topography around the tower are also amply demonstrated. In the final section of this paper, a case study is presented to examine the wind field associated with a typhoon, as well as the characteristics of the ratio of surface to gradient wind speeds $G(r)$ and the inflow angle γ . The results indicate that previous observation data obtained at coastal areas during typhoons can be explained satisfactorily by this model.

Nomenclature

p	pressure, function of r
p_c	central (minimum) pressure
p_w	periphery pressure
Δp	$p_w - p_c$, central pressure difference
B	pressure profile constant

* Corresponding author.

r	radial distance from typhoon center
r_m	radius of maximum winds
v	wind velocity
c	translation velocity of typhoon
f	Coriolis parameter
z_0	equivalent roughness length
d	zero-plane displacement
h	mean height of roughness elements
z, z'	vertical coordinate
z_{10}	height 10 m above the mean height of roughness elements
A	constant
C_d	drag coefficient
$i = \sqrt{-1}$	complex unit
$D = D_1 + iD_2$	complex constant
$G(r)$	ratio of surface to gradient wind speeds
$G(\infty), x_p,$	
$k, G(x_p)$	fitting parameters
β	approach angle, counterclockwise positive from East
θ	angle, counterclockwise positive from East
γ	inflow angle
ρ	air density
k_m	eddy viscosity
$\kappa = 0.40$	Karman constant
ξ, λ	see Eq. (19)
χ	see Eq. (26)

Subscripts

θ	component in the tangential direction
r	component in the radial direction
g	value at the gradient height
s	value on the ground surface

1. Introduction

For wind-resistant structural design, the design wind speed is often determined from statistical probability analysis based on field data. For many coastal regions in Japan, as in most areas on the western rim of the Pacific Ocean, the highest recorded wind speeds are caused by typhoons. Design wind loads for engineering structures in these areas are therefore governed by this factor. In order to reasonably determine design wind loads for such structures by means of standard statistical techniques, at least several decades of annual extreme wind observations would be needed at the proposed construction site. However, such data bases, which would allow

reconstruction of the wind climate caused by typhoons, rarely exist because typhoons are relatively small in size and infrequent in occurrence.

An alternative approach to formulating design wind loads in areas which are dominated by tropical cyclones was first suggested by Russell in 1971 [1] and then developed by a number of researchers [2–6]. The advantage of this approach is that multiple time histories of tropical cyclones in a given locality can be created by computer simulation using the so-called “Monte Carlo” method. These are then used to provide estimates of extreme winds over what are, in effect, long periods of time. Within the simulation, probability distributions of tropical cyclone parameters (such as annual occurrence rate, paths, translation velocity, radius of maximum winds, central pressure difference and decay rate after landfall) are first determined from the observation data, followed by prediction of wind field associated with them. Whether the simulation program is successful depends on two factors: accuracy of the statistical representation of the tropical cyclone parameters; and reliability of the wind field model. The second factor, in particular, influences the results of the simulation.

Several empirical formulas, based on the observation data of typhoons, were formulated in the past to estimate the surface winds of tropical cyclones; see, for example, Refs. [7,8]. Furthermore, Georgiou et al. [3] proposed a model to compute surface wind speeds using an identified relationship between surface and gradient wind speeds. In this model, the gradient wind speed was obtained from the cyclostrophic balance, and the ratio of surface to gradient wind speeds, $G(r)$, was determined from the observation data. Afterwards, Fujii and Mitsuda [6] expressed the ratio $G(r)$ as a function of the distance r . The fitting parameters included in the function were identified from the wind speed data of two typhoons observed in the southwest islands in 1977. However, the physical features of the typhoon boundary layer and the surface terrain conditions were not considered, a problem common to empirical models.

Instead of proposing empirical formulas or models through use of the observation data obtained from typhoons or hurricanes, Yoshizumi [9] derived an analytical solution from the Navier–Stokes equation. He assumed that the gradient wind velocity was expressed through the addition of the translation velocity of the typhoon and the wind velocity relative to the storm center. The surface wind velocity was obtained using the approximate solution of Rosenthal [11]. However, the typhoon-induced wind speeds computed by the analytical solution tend to be underestimated on the left side. In the particular case of a typhoon with a high translation velocity, the wind speed distribution on the left side of the typhoon was unrealistic.

This paper presents a new analytical model for the prediction of the typhoon-induced wind field. It involves modeling of wind field generated by moving typhoons and the concept of the so-called “equivalent roughness length” for evaluating terrain roughness and topographical effect. The observed wind speed and direction records obtained from three typhoons in 1991 are compared with those computed by the new analytical model to confirm the model validity. A comparison of the typhoon models is then performed to clarify problems with empirical wind speed models. Finally, the wind field generated by a typhoon, as well as the characteristics of the wind speed ratio and inflow angle, are investigated using the present model.

2. An analytical solution for typhoon-induced wind field

2.1. Model

It is well known that the pressure isobars in the domain of a typhoon are distributed in approximately concentric circles with respect to the center of the typhoon. This pressure is usually computed from the relationship proposed by Holland [11],

$$p = p_c + \Delta p \exp[-(r_m/r)^B]. \quad (1)$$

In the case of $B = 1.0$, this relationship becomes the Schloemer empirical formula [12]. Considering that the strong wind field in a lower typhoon boundary layer is in a neutral condition [13], the equation of motion can be written as

$$\frac{\partial \mathbf{v}}{\partial t} + \mathbf{v} \cdot \nabla \mathbf{v} = -\frac{1}{\rho} \nabla p - f \mathbf{k} \times \mathbf{v} + \mathbf{F}. \quad (2)$$

Because the vertical scale of the typhoon (10 km) is much less than its horizontal scale (1000 km), the hydrostatic approximation is valid. In this study, the typhoon-induced wind velocity \mathbf{v} is expressed by the addition of the gradient wind \mathbf{v}_g in the free atmosphere (called GW hereafter), and the component \mathbf{v}' , caused by the friction on the ground surface, as

$$\mathbf{v} = \mathbf{v}_g + \mathbf{v}'. \quad (3)$$

Since the radial pressure gradient does not vary with height in the lower typhoon boundary layer, and the frictional force \mathbf{F} is negligible above the boundary layer, the equation of motion (2) can be divided into the following two formulas,

$$\frac{\partial \mathbf{v}_g}{\partial t} + \mathbf{v}_g \cdot \nabla \mathbf{v}_g = -\frac{1}{\rho} \nabla p - f \mathbf{k} \times \mathbf{v}_g. \quad (4)$$

$$\frac{\partial \mathbf{v}'}{\partial t} + \mathbf{v}' \cdot \nabla \mathbf{v}' + \mathbf{v}' \cdot \nabla \mathbf{v}_g + \mathbf{v}_g \cdot \nabla \mathbf{v}' = -f \mathbf{k} \times \mathbf{v}' + \mathbf{F}. \quad (5)$$

In order to analytically solve Eqs. (4) and (5), modeling of the unsteady terms in these equations is carried out as follows: (a) In the free atmosphere, the gradient wind pattern \mathbf{v}_g moves at the translation velocity of the typhoon \mathbf{c} . Therefore, the unsteady term in Eq. (4) becomes

$$\frac{\partial \mathbf{v}_g}{\partial t} = -\mathbf{c} \cdot \nabla \mathbf{v}_g. \quad (6)$$

(b) In the typhoon boundary layer, the unsteady term in Eq. (5) is considered smaller than the viscosity term and the inertia term, and is disregarded as

$$\frac{\partial \mathbf{v}'}{\partial t} = 0. \quad (7)$$

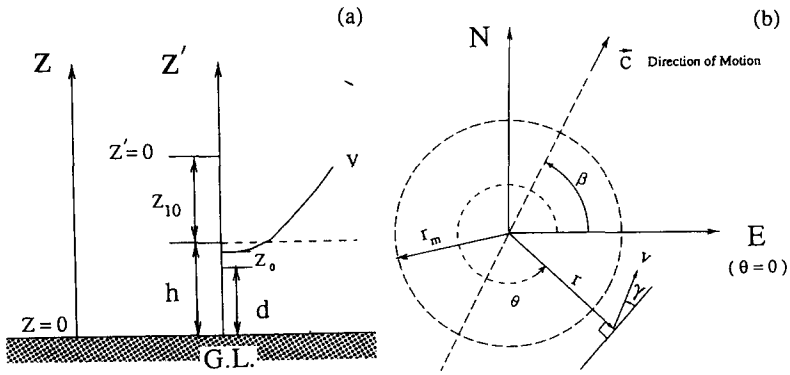


Fig. 1. Coordinate system. (a) Vertical direction; (b) horizontal direction.

Consequently, Eqs. (4) and (5) become

$$(\mathbf{v}_g - \mathbf{c}) \cdot \nabla \mathbf{v}_g = -\frac{1}{\rho} \nabla p - f \mathbf{k} \times \mathbf{v}_g, \tag{8}$$

$$\mathbf{v}' \cdot \nabla \mathbf{v}' + \mathbf{v}' \cdot \nabla \mathbf{v}_g + \mathbf{v}_g \cdot \nabla \mathbf{v}' = -f \mathbf{k} \times \mathbf{v}' + \mathbf{F}. \tag{9}$$

The boundary condition at the upper atmosphere is

$$\mathbf{v}'|_{z' \rightarrow \infty} = 0. \tag{10}$$

Above the ground surface, the boundary condition that shearing stress balances with drag force is

$$\rho k_m \left. \frac{\partial \mathbf{v}'}{\partial z} \right|_{z'=0} = \rho C_d |\mathbf{v}_s| \mathbf{v}_s, \tag{11}$$

where \$z\$ indicates the vertical axis as shown in Fig. 1 and \$z = 0\$ is set on the ground surface. On the assumption that the wind speed profile in the vicinity of the ground surface is logarithmic, the relationship between \$C_d\$ and the roughness length \$z_0\$ becomes

$$C_d = \kappa^2 / \{ \ln[(z_{10} + h - d)/z_0] \}^2, \tag{12}$$

where the zero-plane displacement is derived from \$d = 0.75h\$ [14] and the mean height of the roughness elements \$h\$ is expressed through the use of the equation \$h = Az_0^{0.86}\$ proposed by Lettau [15]. The value of \$A\$ is identified to be 11.4 from the observation data obtained by Helliwell [16], and Kondo and Yamazawa [17]. The value for \$z_{10}\$ is set at a height of 10 m above the mean height of the roughness element. The height for \$z' = 0\$ is placed at \$h + z_{10}\$ which is the base of the computation domain.

2.2. *Wind velocity field in the free atmosphere*

Since the pressure isobars in the domain of a moving typhoon are axisymmetrical with respect to the center of the typhoon, the cylindrical coordinate system is used, and Eq. (8) is written as

$$(v_{rg} - c_r) \frac{\partial v_{rg}}{\partial r} + \frac{v_{\theta g} - c_\theta}{r} \frac{\partial v_{rg}}{\partial \theta} - \frac{v_{\theta g}^2}{r} + \frac{v_{\theta g} c_\theta}{r} = -\frac{1}{\rho} \frac{\partial p}{\partial r} + f v_{\theta g}, \tag{13}$$

$$(v_{rg} - c_r) \frac{\partial v_{\theta g}}{\partial r} + \frac{v_{\theta g} - c_\theta}{r} \frac{\partial v_{\theta g}}{\partial \theta} + \frac{v_{\theta g} v_{rg}}{r} - \frac{v_{rg} c_\theta}{r} = -f v_{rg}, \tag{14}$$

where $c_r = c \cos(\theta - \beta)$ and $c_\theta = -c \sin(\theta - \beta)$. Considering that the radial velocity v_{rg} is smaller than the tangential velocity $v_{\theta g}$ in the free atmosphere, the first and second convection terms on the left-hand side of Eq. (13) are disregarded. The wind velocity $v_{\theta g}$ is expressed approximately as

$$v_{\theta g} = \frac{1}{2} (c_\theta - fr) + \left[\left(\frac{c_\theta - fr}{2} \right)^2 + \frac{r}{\rho} \frac{\partial p}{\partial r} \right]^{1/2}. \tag{15}$$

This expression of the gradient wind field has the same form as that obtained from the equation of cyclostrophic balance in which the centrifugal acceleration, in the presence of general typhoon translation, is calculated using Blaton’s formula. The radial velocity v_{rg} can be obtained from the equation of continuity as follows,

$$v_{rg} = -\frac{1}{r} \int_0^r \frac{\partial v_{\theta g}}{\partial \theta} dr. \tag{16}$$

Considering approximate accuracy v_{rg} is set at 0 in this study.

2.3. *Velocity component v' caused by ground surface friction*

Perturbation analysis is performed to obtain the distribution of \mathbf{v}' in the vertical direction. The velocity components of v'_θ , v'_r are assumed to be small compared with the gradient wind, and the first derivative of the velocity components with respect to θ are presumably small compared with the velocity components. The equation of motion (9) can be linearized with these considerations as

$$-\left(2 \frac{v_{\theta g}}{r} + f \right) v'_\theta = k_m \frac{\partial^2 v'_r}{\partial z^2}, \tag{17}$$

$$\left(\frac{\partial v_{\theta g}}{\partial r} + \frac{v_{\theta g}}{r} + f \right) v'_r = k_m \frac{\partial^2 v'_\theta}{\partial z^2}. \tag{18}$$

Introducing the following two abbreviations,

$$\begin{aligned} \xi &= \left(\frac{\partial v_{\theta g}}{\partial r} + \frac{v_{\theta g}}{r} + f \right)^{1/2} \left/ (2v_{\theta g}/r + f)^{1/2}, \right. \\ \lambda &= \left(\frac{\partial v_{\theta g}}{\partial r} + \frac{v_{\theta g}}{r} + f \right)^{1/4} \left(2 \frac{v_{\theta g}}{r} + f \right)^{1/4} \left/ (2k_m)^{1/2}, \right. \end{aligned} \tag{19}$$

and rearranging Eqs. (17) and (18) gives

$$2\lambda^2 v''_{\theta} = \frac{\partial^2 v''_r}{\partial z^2}, \tag{20}$$

$$- 2\lambda^2 v''_r = \frac{\partial^2 v''_{\theta}}{\partial z^2}, \tag{21}$$

where $v''_{\theta} = v'_{\theta}$ and $v''_r = -v'_r/\xi$. Multiplication of Eq. (20) by i and addition of the result to Eq. (21) produces

$$\frac{\partial^2 \mathbf{v}''}{\partial z^2} - [(1 + i)\lambda]^2 \mathbf{v}'' = 0, \tag{22}$$

and the solution satisfying the boundary condition (10) is

$$\mathbf{v}'' = \mathbf{D} \exp[-(1 + i)\lambda z'], \tag{23}$$

where $\mathbf{D} (= D_1 + iD_2)$ is a complex constant found from the boundary condition above the ground surface. The velocity components are obtained as

$$v'_{\theta} = e^{-\lambda z'} [D_1 \cos(\lambda z') + D_2 \sin(\lambda z')], \tag{24}$$

$$v'_r = -\xi e^{-\lambda z'} [D_2 \cos(\lambda z') - D_1 \sin(\lambda z')], \tag{25}$$

where

$$\begin{aligned} D_1 &= -\frac{\chi(\chi + 1)v_{\theta g} - \chi v_{rg}/\xi}{1 + (\chi + 1)^2}, \\ D_2 &= \frac{\chi v_{\theta g} + \chi(\chi + 1)v_{rg}/\xi}{1 + (\chi + 1)^2}, \\ \chi &= \frac{C_d}{k_m \lambda} |\mathbf{v}_s| = \frac{C_d}{k_m \lambda} \sqrt{v_{\theta s}^2 + v_{rs}^2}. \end{aligned} \tag{26}$$

Since \mathbf{v}_s is included in the formula of χ , the value of v_{θ} , v_r must be found from iterated computation. The gradient wind velocities of $v_{\theta g}$, v_{rg} are used for the initial value of $v_{\theta s}$, v_{rs} . The eddy viscosity is fixed at 100 m²/s in reference to the value [18,9] obtained from hurricane observation. The air density ρ is set at 1.2 N s²/m⁴.

3. An application for simulating three typhoons

The wind records resulting from three typhoons – Caitlin, Kinna, Mireille (Fig. 2) – are simulated to confirm the validity of the present model.

Typhoon Caitlin (T9109) passed through the left-hand side of the observation site on 29 July. Typhoon Kinna (T9117) traveled over the right hand side of the site on 14 September. Typhoon Mireille (T9119), the strongest, passed over the site at 16:00 JST on 27 September, devastating the Japanese islands during 27, 28 September at tremendous speed. Records for maximum wind speed were set at many meteorological stations located in Kyusyu districts, western Japan and Tohoku districts. The parameters of the three typhoons, except for the value of r_m , have been obtained from the Japanese Meteorological Agency and are summarized in Table 1. An optimum fit of r_m by the least squares method using Eq. (1) was obtained using the central pressure p_c and the central pressure difference Δp . The best overall fit for the three typhoons is given by a value of $B = 1.0$.

Wind speed and direction records (10 min mean) were obtained from a 100 m observation tower located at the center of the Huis Ten Bosch [19]. Wind speed and direction were measured using a three-cap anemometer (AF-860, Makino Applied Instruments Inc.) and a wind vane (VF-216, Makino Applied Instruments Inc.), both of which were installed at the top of the tower. The resolution of the wind vane is 22.5° .

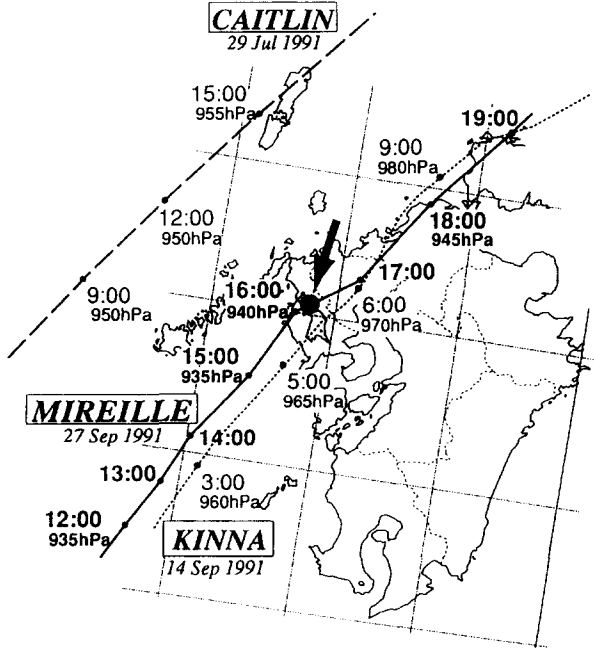


Fig. 2. The tracks of Typhoons Caitlin (T9109), Kinna (T9117), Mireille (T9119).

Table 1
Summary of the parameters used in the three typhoon simulations

Name	Date (J.S.T)	Time (J.S.T.)	Latitude (deg)	Longitude (deg)	β (deg)	C (m/s)	p_c (hPa)	Δp (hPa)	r_m (km)
T9109	91.07.29	8	32.8	127.8	55.31	7.51	948.3	64.7	87.88
		9	33.0	128.0	54.56	7.58	950.0	63.0	83.45
		10	33.2	128.2	55.43	7.50	950.0	63.0	79.11
		11	33.4	128.3	55.49	7.49	950.0	63.0	78.79
		12	33.6	128.5	54.43	8.16	950.0	63.0	79.33
		13	33.8	128.7	54.80	8.88	951.7	61.3	82.60
		14	34.1	128.9	54.87	8.87	953.3	59.7	87.79
		15	34.3	129.1	52.25	9.77	955.0	58.0	88.95
		16	34.6	129.4	50.60	10.60	956.7	56.3	77.25
		17	34.8	129.6	50.70	10.58	958.3	54.7	83.69
18	35.1	129.9	52.92	10.46	960.0	53.0	91.32		
T9117	91.09.14	0	30.9	128.7	70.58	10.30	955.0	58.0	43.36
		1	31.2	128.8	71.02	10.92	956.7	56.3	48.26
		2	31.6	129.0	71.08	10.91	958.3	54.7	49.90
		3	31.9	129.1	63.51	12.58	960.0	53.0	55.56
		4	32.3	129.4	57.71	14.61	962.5	50.5	55.36
		5	32.7	129.7	53.74	15.32	965.0	48.0	51.09
		6	33.1	130.1	55.51	13.68	970.0	43.0	56.19
		7	33.4	130.3	63.57	11.54	973.3	39.7	57.24
		8	33.8	130.5	63.66	11.53	976.7	36.3	62.30
		9	34.1	130.7	43.98	14.71	980.0	33.0	65.62
10	34.4	131.3	32.78	19.22	981.7	31.3	73.72		
T9119	91.09.27	10	30.3	127.9	62.33	15.15	935.0	78.0	67.06
		11	30.8	128.1	62.44	15.13	935.0	78.0	71.78
		12	31.2	128.4	60.53	15.24	935.0	78.0	75.12
		13	31.6	128.7	59.66	15.55	935.0	78.0	77.97
		14	32.1	129.0	59.78	15.54	935.0	78.0	77.20
		15	32.5	129.3	51.12	14.49	935.0	78.0	77.96
		16	32.8	129.7	50.09	17.13	940.0	73.0	84.43
		17	33.4	130.2	55.77	20.55	942.5	70.5	88.65
		18	33.9	130.6	52.06	21.17	945.0	68.0	89.53
		19	34.4	131.2	49.10	21.90	945.0	68.0	87.33
20	35.0	131.7	42.29	21.84	945.0	68.0	88.13		

The observed wind speeds and directions for the three typhoons have been compared with those obtained using the present model in Figs. 3a–3c. The dotted and the broken lines show the results, computed using different roughness lengths z_0 . It should be noted that the values of the wind speeds depend on the value of z_0 .

In the case of Typhoon Caitlin (T9109), the computed curve where $z_0 = 0.07$ m corresponds well with the observed data during the period before 12:00. However, the computed curve where $z_0 = 0.5$ m coincides with the observed data after 13:00. Note from Fig. 3a that a rapid decrease in wind speed occurred when the wind direction exceeded 180° .

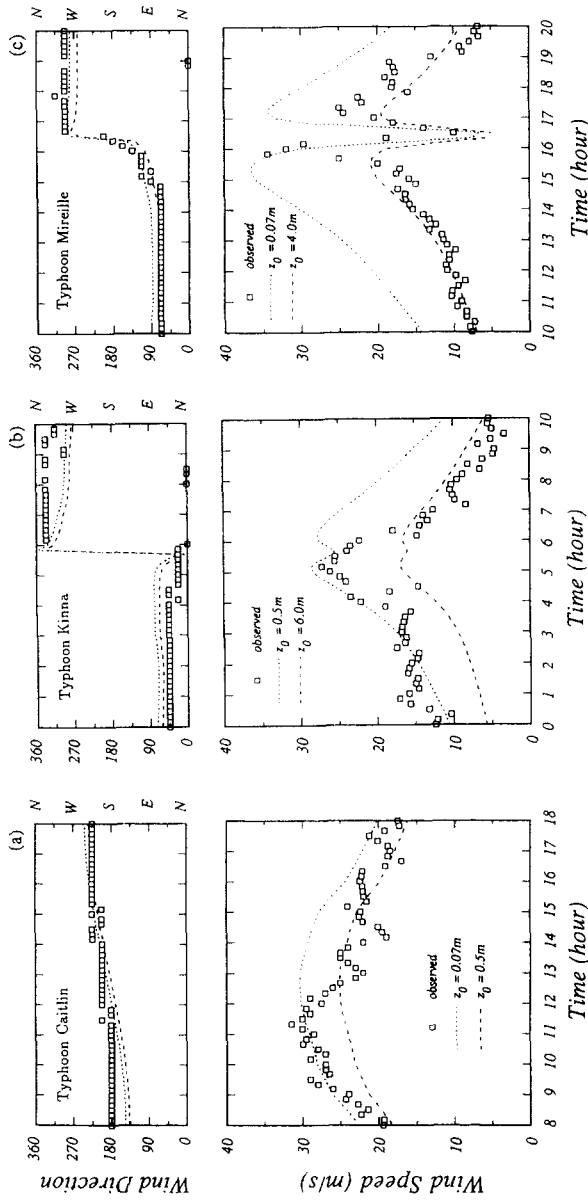


Fig. 3. Time variations of the computed and observed wind speeds and directions. (a) Typhoon Caitlin; (b) Typhoon Kinna; (c) Typhoon Mireille.

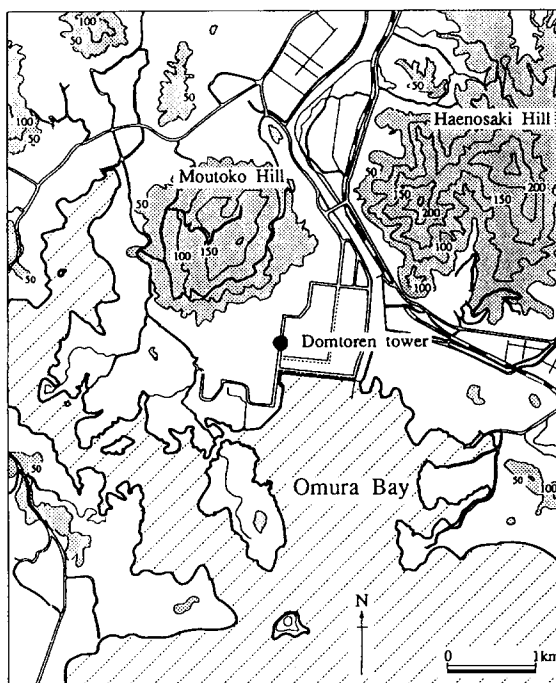


Fig. 4. Topography around the observation site. The shadowed areas are higher than 50 m.

With regard to Typhoon Kinna (T9117), the calculated curve where $z_0 = 0.5$ m corresponds to the observation data before 6:00. However, the calculated curve where $z_0 = 6.0$ m coincides with the observation data during the period after 6:00. During particularly strong winds, the wind direction ranged between 0° and 30° .

Regarding Typhoon Mireille (T9119), although the value obtained using $z_0 = 4.0$ m corresponds to observation values before 15:30, the data observed during the period from 15:40 to 16:20 corresponds well with the results computed using $z_0 = 0.07$ m. It should be noted from Fig. 3c that the wind speed changed rapidly when the wind direction exceeded 90° .

In the aforementioned cases, it is obvious that the roughness lengths at the Huis Ten Bosch depend on the wind direction. Fig. 4 shows the topography of the Huis Ten Bosch, in which the shadowed areas have elevations of 50 m or more. The southeast portion of the site is Omura Bay, where the roughness is smaller. The roughness length $z_0 = 0.07$ m for this direction appears reasonable. On the other hand, both the northeast and northwest areas of the site are surrounded by hills higher than 150 m. The winds blowing from these two directions were weak because of the influence of these topographies. It can also be understood that the wind blowing from the directions between 0° and 30° is appropriately simulated using $z_0 = 0.5$ m, because the areas in these directions are flat surfaces.

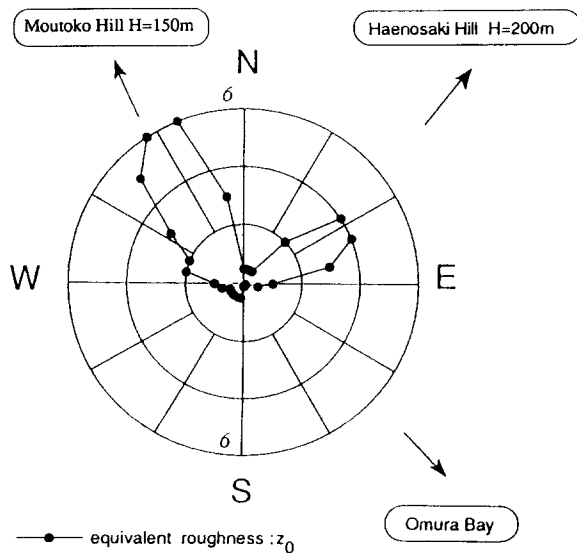


Fig. 5. Polar diagram of equivalent roughness z_0 at the Huis Ten Bosch.

Table 2
Roughness length z_0 (m) in previous proposals and loading codes

Terrain category	Ref. [20]	Ref. [21]	Ref. [22]	Ref. [23]	Ref. [24]
I	0.0002–0.004	0.0004–0.02	0.0002–0.006	0.005	0.0005–0.04
II	0.01–0.06	0.001–0.2	0.03–0.17	0.07	0.003–0.2
III	0.2–0.9	1.0–1.5	0.24–0.75	0.3	0.1–1.0
IV	1.0–5.0	1.0–4.0	1.12	1.0	0.4–2.0
V	1.0–5.0	1.0–4.0	1.6	1.5	1.5–4.0

In this study, the topographical effect is regarded as the equivalent terrain roughness, and both the topographical effect and terrain roughness are expressed by a single bulk parameter of z_0 . For expanding the conventional definition of the roughness length, the parameter z_0 is here referred to as the equivalent roughness length. Fig. 5 illustrates the polar diagram of the equivalent roughness z_0 identified from the observation data. The values of z_0 in the northeast and northwest directions are very large ($z_0 = 4.0\text{--}6.0\text{ m}$) owing to the influence of the hills. The values in the other directions correspond to the results of past studies, as shown in Table 2 (see, e.g., Refs. [20–24]).

Figs. 6a–6c show the wind directions and speeds of the three typhoons calculated by using the identified value of z_0 . The predicted values agree favorably with the observation data. This indicates that if the value of z_0 in every wind direction is identified from observations or wind tunnel tests, a typhoon-induced wind field can be

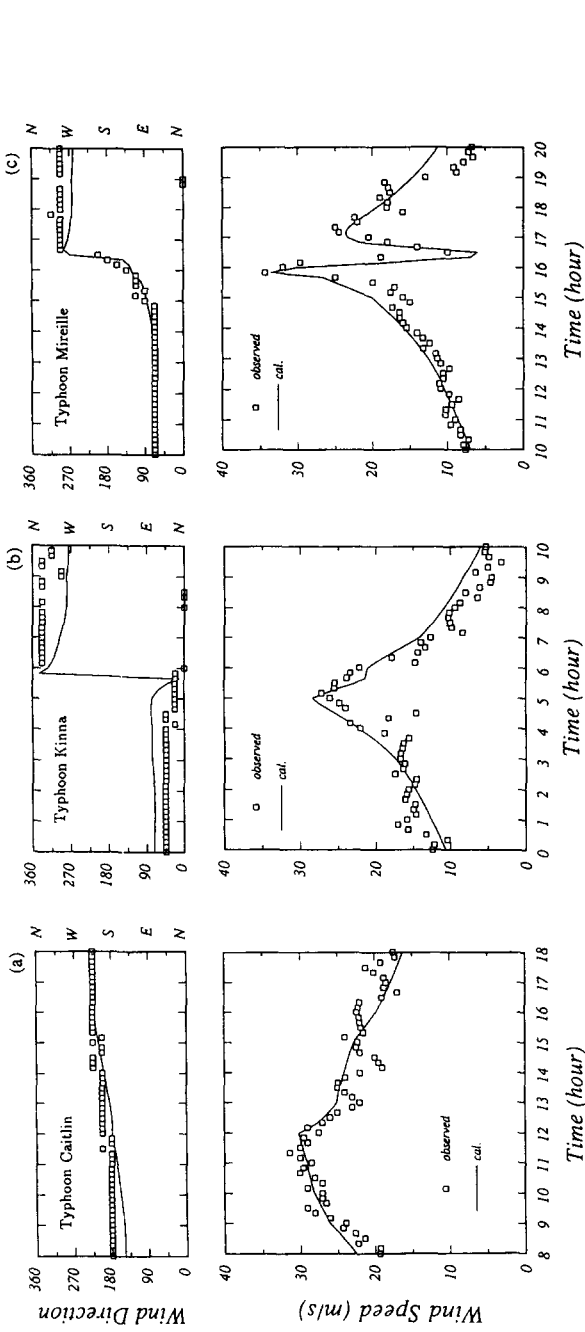


Fig. 6. Time variations of wind speeds and directions computed by using the calibrated equivalent roughness z_0 . (a) Typhoon Caitlin; (b) Typhoon Kinna; (c) Typhoon Miraille.

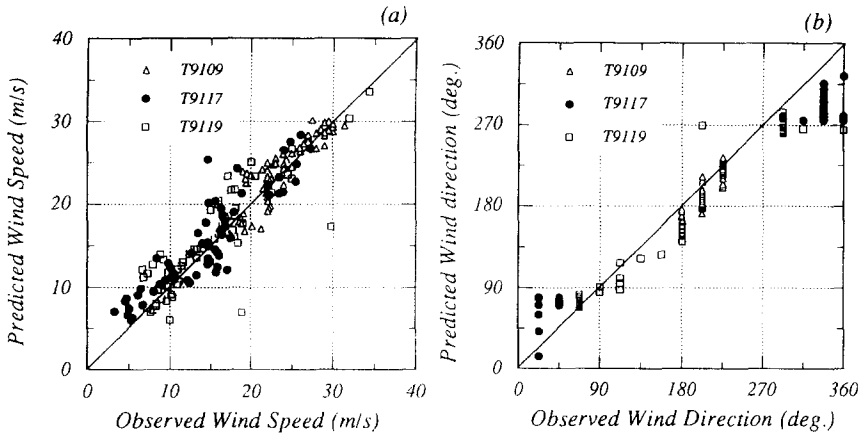


Fig. 7. Comparison of wind speeds and directions computed by using the present model and observed data.

accurately simulated. Figs. 7a, 7b show a comparison of wind speeds and directions computed by the present model and observed data. The correlation coefficients on wind speed and direction are 0.93 and 0.98, respectively, as seen in Figs. 7a, 7b. The validity of the model is confirmed.

4. Comparison with other typhoon models

The typhoon models were compared in order to clarify differences between the present model and the empirical model proposed by Georgiou et al. [3]. With regard to the ratio $G(r)$ of surface to gradient wind speeds, the equation proposed by Fujii and Mitsuta (called the FM model hereafter) was used, in which the wind speed ratio $G(x) = v_s/v_g$ is assumed to be a function of $x = r/r_m$ and is written as

$$G(x) = G(\infty) + [G(x_p) - G(\infty)] \left(\frac{x}{x_p} \right)^{k-1} \exp\{ (1 - 1/k) [1 - (x/x_p)^k] \}. \quad (27)$$

The inflow angle γ is set at 30° . Detailed explanations of the FM model are described in Ref. [6]. The wind speed data from Typhoon Mireille (T9119) have been used for comparison of the typhoon models. The best overall fit for the surface wind obtained from Typhoon Mireille is given by the following values: $G(\infty) = 0.6$, $x_p = 0.5$, $G(x_p) = 1.0$, $k = 2.5$.

Fig. 8 illustrates the calculated radial distribution of wind speed using the FM model. The squares and circles represent the data obtained at the front and rear sides of the center of the typhoon. The computed curve appears to provide the best overall fit for the surface wind. Fig. 9 shows the time variation of wind speed and direction

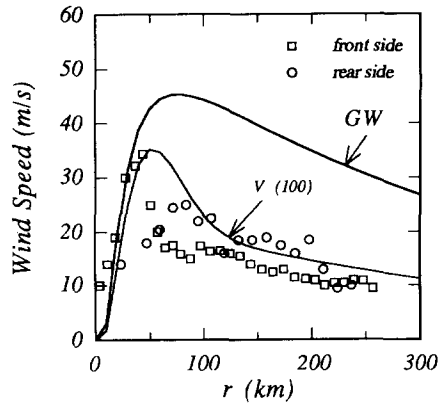


Fig. 8. The radial distribution of wind speed for Typhoon Mireille (T9119); symbols: observed; solid line: simulated using the FM model.

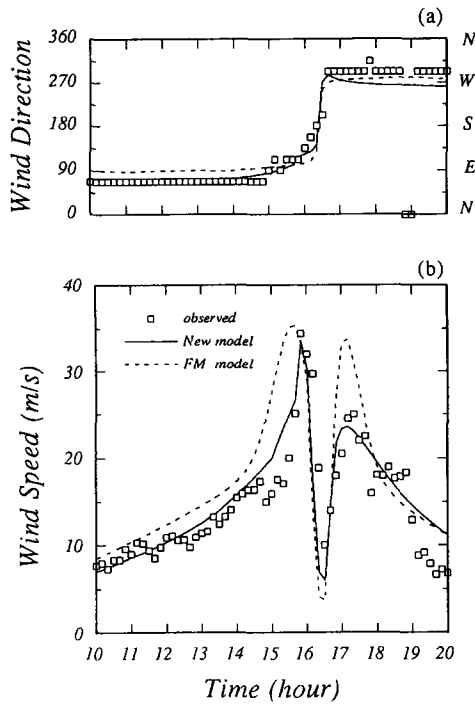


Fig. 9. Comparison of the time variation of the wind direction (a) and speed (b) computed by the FM model and the present model.

computed by the FM model and the present model, as well as the observation data. Although there is little difference between the models with regard to wind direction, the wind speed calculated after 16:00 by the FM model is overestimated. It is obvious in this case that the wind speed ratio depends not only on the radial distance from the typhoon center but also on the wind direction, because of the heterogeneity of surface roughness and topography around the observation site.

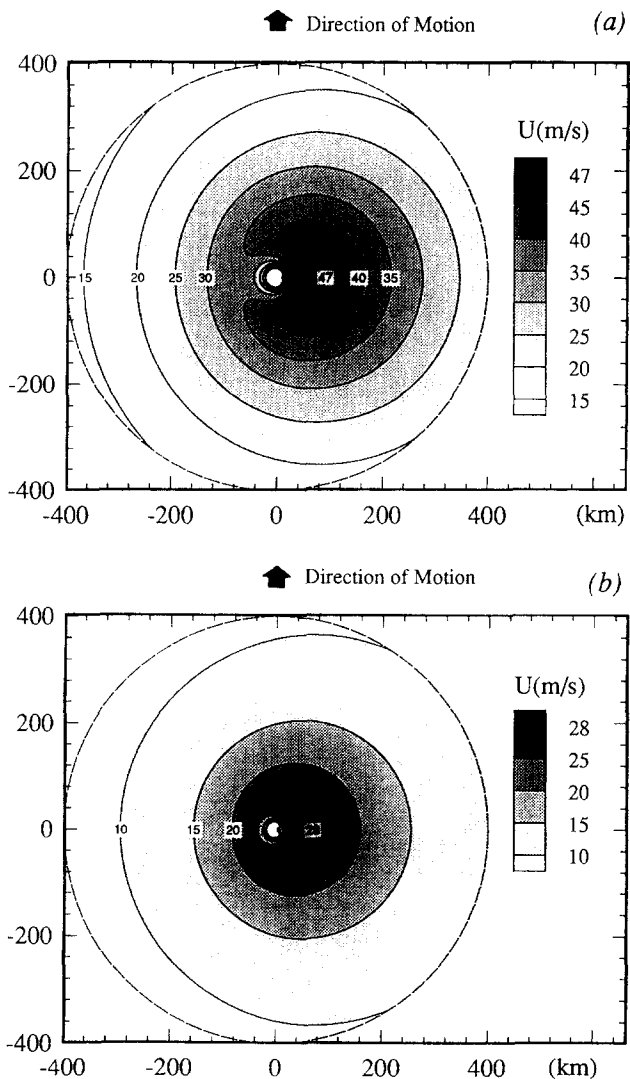


Fig. 10. Contours of wind speed calculated using the present model. (a) Gradient wind speed; (b) surface wind speed.

5. Wind speed ratio $G(r)$ and inflow angle γ

It is well known that the wind speed ratio $G(r)$ tends to be almost constant when the center of a typhoon moves away from an observation point at coastal areas. It has been reported that the value of $G(\infty)$ is within 0.45–0.67 [3,6], and that the inflow angle γ shows a value close to 30° . Theoretical explanations of these observation results have seldom been given.

To examine the characteristics of both the wind speed ratio $G(r)$ and the inflow angle γ , a case study was analyzed using the present model. In relation to the data of the three typhoons analyzed in Section 3, $\Delta p = 60$ hpa, $r_m = 80$ km, $c = 15$ m/s, $z_0 = 0.1$ m were selected as typhoon parameters.

Fig. 10a illustrates the contours of the gradient wind speed. The maximum wind velocity is shown at the point $r = r_m$ and the difference in the maximum wind velocity between the right- and the left-hand side for the movement direction is almost equivalent to the magnitude of the translation velocity c . Fig. 10b shows the contours of the surface wind speed. The maximum value of the surface wind velocity is found inside the radius of maximum wind, as is often observed in surface wind data during a typhoon. Fig. 11 plots the velocity vectors and streamlines on the surface. A fairly strong convergent flow exists in the vicinity of the ground surface, which causes the transport of momentum in the radial direction owing to the existence of spatial heterogeneity of the wind field in the typhoon boundary layer.

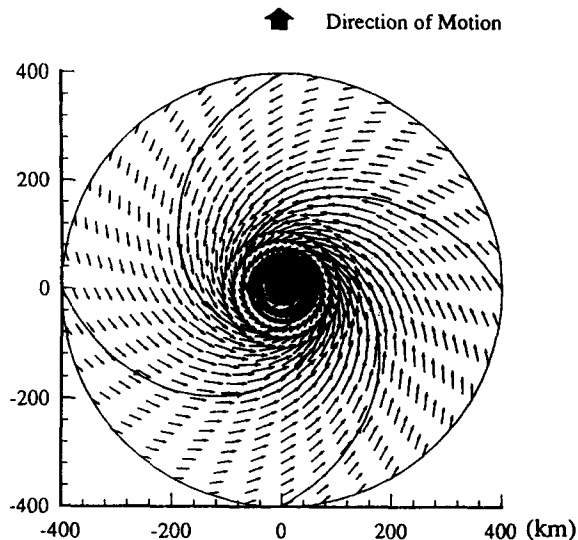


Fig. 11. Velocity vectors v_θ, v_r on the surface calculated using the present model. Streamlines are also presented.

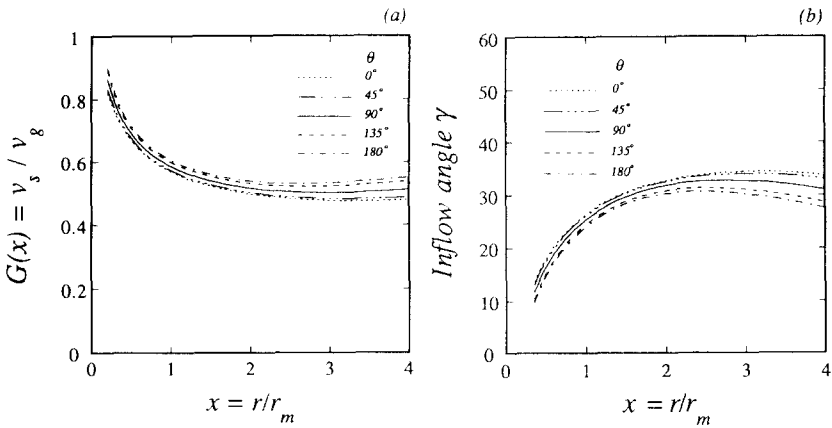


Fig. 12. (a) Wind speed ratio $G(r)$ and (b) inflow angle γ in various orientations calculated using the present model.

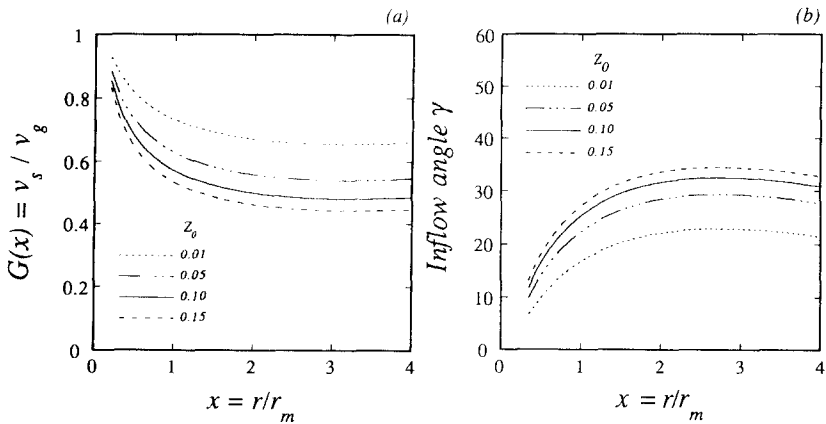


Fig. 13. (a) Averaged wind speed ratio $G(r)$ and (b) averaged inflow angle γ calculated using various z_0 .

Using these results, the wind speed ratio $G(r)$ and the inflow angle γ in a radial direction for various orientations have been calculated and the results are shown in Figs. 12a, 12b. At places located away from the center of the typhoon, $G(r)$ shows almost constant values, and γ presents a value close to 30° . Although their values depend on the orientation, the range of variation is fairly small. Variations due to a difference of orientation are thought to be caused by the nonlinear effect of the boundary condition on the ground surface.

Finally, variations of $G(r)$ and γ with a roughness length of z_0 are investigated using the same typhoon parameters. Figs. 13a, 13b show the averaged $G(r)$ and averaged γ for all orientations. The curves in Fig. 13 represent the results calculated using $z_0 = 0.01, 0.05, 0.1$ and 0.15 m. The values of $G(r)$ decrease as z_0 increases. This is

because the surface wind speed decreases with surface roughness increase. The variation of the observation data on $G(\infty)$ is explained by a change in surface roughness. The value of the inflow angle γ also depends on the surface roughness and increases as z_0 increases. The inflow angle does not vary rapidly and shows a value of approximately 30° at most places except in the vicinity of the center of the typhoon. The results satisfactorily explain past observations at coastal areas.

6. Conclusions

An analytical model has been presented for the prediction of typhoon-induced wind field. The model has been applied to three typhoons observed in 1991 at a 100 m tower at Nagasaki, Japan. The wind speeds and directions computed by the present model agree favorably with those observed. In this study, the concept of the so-called “equivalent roughness length” was introduced to evaluate the terrain roughness and topographical effect. Using this single-bulk parameter, it is possible to simulate surface wind speed as well as wind direction at a site with complex terrain conditions.

The model has been shown to be superior to the widely used empirical model. It provides more accurate predicted wind speeds at a site with complex terrain conditions than the empirical model which overestimates wind speeds in some wind direction. This indicates that the wind speed ratio depends not only on the radius distance from the typhoon center but also on the wind direction, because of the heterogeneity of surface roughness and topography around the observation site.

A typhoon-induced wind field simulated by the model was presented in the final section of this paper. The maximum wind speed in the free atmosphere is shown at the point $r = r_m$ on the right-hand side of the typhoon, but the maximum value of the surface wind speed is found inside the radius of maximum wind. Characteristics of the wind speed ratio $G(r)$ and the inflow angle γ were also investigated. The results indicate that the model satisfactorily explains past observation data obtained at coastal areas.

Acknowledgement

The authors express their gratitude to Dr. Yukio Tamura, Professor at Tokyo Polytechnic University, and Mr. Kenji Shimada, researcher at the Institute of Technology of Shimizu Corporation, for providing valuable typhoon observation data.

References

- [1] L.R. Russell, Probability distributions for hurricane effects, J. of the Waterways, Harbor and Coastal Engineering Division, ASCE, Vol. 97, No. WW1, Proc. Paper 7886, February, 1971, pp. 139–154.
- [2] B.V. Tryggvason, D. Surry and A.G. Davenport, Predicting wind induced response in hurricane zones, J. of the Structural Division, ASCE, Vol. 102, No. ST12, Proc. Paper 12630, December, 1976, pp. 2333–2350.

- [3] P.N. Georgiou, A.G. Davenport and B.J. Vickery, Design wind speeds in regions dominated by tropical cyclones, *J. Wind Eng. Ind. Aerodyn.* 13 (1983) 139–152.
- [4] M.E. Batts, M.R. Cordes, L.R. Russell, J.R. Shaver and E. Simiu, Hurricane wind speeds in the U.S.A., NBS Building Science series 124 (National Bureau of Standards, Washington, 1980).
- [5] G.S. Martin, Probability distributions for hurricane wind gust speeds on the Australian Coast, in: Proc. I.E. Aust. Conf. on Applied probability theory to structural design, Melbourne, 1974.
- [6] T. Fujii and Y. Mitsuta, Simulation of winds in typhoons by a stochastic model, *J. Wind Eng. No. 28* (1986) 1–12 [in Japanese].
- [7] K. Terada and J. Kondo, Trajectory of air parcel and energy supply from the ocean in typhoon area, *Sea and Air* 48, No. 1 (1972) 1–14.
- [8] Y. Mitsuta, T. Fujii and O. Tsukamoto, Simulation of the surface wind in typhoon, *Annuals of Disaster Prevention Research Institute, Kyoto University* Vol. 25B1 (1982) 273–282 [in Japanese].
- [9] S. Yoshizumi, On the asymmetry of wind distribution in the lower layer of a typhoon, *J. Meteor. Soc. Japan* 46, No. 3, (1968) 153–159.
- [10] S.L. Rosenthal, A theoretical analysis of the field of motion in the hurricane boundary layer, National Hurricane Research Project Report, No. 56 (1962) 12 pp.
- [11] G.J. Holland, An analytic model of the wind and pressure profiles in Hurricanes, *Mon. Weather Rev.* 108 No. 8 (1980) 1212–1218.
- [12] R.W. Schloemer, Analysis and synthesis of hurricane wind patterns over Okeechobee, Florida, Hydrometeorological Report, No. 31 (1954) 49 pp.
- [13] Y. Meng, M. Matsui and K. Hibi, A theoretical analysis of the wind field in the typhoon boundary layer, *J. Wind Eng. No. 55* (1993) 7,8 [in Japanese].
- [14] E. Simiu, Equivalent static wind load for tall building design, in: Proc. 4th ICWE (Cambridge Univ. Press, Cambridge, 1977) pp. 721–733.
- [15] H.H. Lettau, Physical and meteorological basis for mathematical models of urban diffusion processes, in: Proc. Symp. on Multiple-source urban diffusion models, U.S. EPA, Publ. AP-86 Research Triangle Park, N.C., 1970, pp. 2.1–2.26.
- [16] N.C. Helliwell, Wind over London, in: Proc. Wind effects on buildings and structures, Tokyo, 1971, pp. 23–32.
- [17] J. Kondo and H. Yamazawa, Aerodynamic roughness over an inhomogeneous ground surface, *Bound.-Layer Meteorol.* 35 (1986) 331–348.
- [18] R.K. Smith, The surface boundary layer of a hurricane, *Tellus*, Vol. 20 (Almquist and Wiksell, Stockholm, 1968) pp. 473–484.
- [19] Y. Tamura, K. Shimada and K. Hibi, Wind Response of a tower (Typhoon observation at the Nagasaki Huis Ten Bosch Domtoren), *J. Wind Eng. Ind. Aerodyn.* 50 (1993) 309–318.
- [20] A.G. Davenport, The relationship of wind structure to wind loading, in: Proc. Symp. No. 16, on Wind effects on building and structures, Nat. Phys. Lab., 1963, H.M.S.O., 1965, pp. 54–102.
- [21] J. Counihan, Adiabatic atmospheric boundary layers. A review and analysis of data from the period 1880–1972, *Atmos. Environ.* 9 (1975) 871–905.
- [22] J. Wieringa, Roughness-dependence geographical interpolation of surface wind averages, *Q. J. R. Meteorol. Soc.* 112 (1986) 867–889.
- [23] ECCS: Recommendations for calculating the effects of wind on constructions, 2nd Ed., Technical Committee 12, No. 52, ECCS (1987).
- [24] H. Choi and J. Kanda, Characteristics of the vertical wind profile for wind load estimation, *J. Wind Eng. No. 45* (1990) 23–43 [in Japanese].